



# Fabrication of AA2024–TiO<sub>2</sub> nanocomposites through stir casting process

Mehrdad SHAYAN<sup>1</sup>, Beitallah EGHBALI<sup>1</sup>, Behzad NIROUMAND<sup>2</sup>

1. Department of Materials Science and Engineering, Sahand University of Technology,  
P. O. Box 51335-1996, Tabriz, Iran;

2. Department of Materials Engineering, Isfahan University of Technology, Isfahan 84156-83111, Iran

Received 19 December 2019; accepted 28 September 2020

**Abstract:** Given the nonuse of TiO<sub>2</sub> nanoparticles as the reinforcement of AA2024 alloy in fabricating composites by ex-situ casting methods, it was decided to process the AA2024–*x*TiO<sub>2(np)</sub> (*x*=0, 0.5 and 1 vol.%) nanocomposites by employing the stir casting method. The structural properties of the produced samples were then investigated by optical microscopy and scanning electron microscopy; their mechanical properties were also addressed by hardness and tensile tests. The results showed that adding 1 vol.% TiO<sub>2</sub> nanoparticles reduced the grain size and dendrite arm spacing by about 66% and 31%, respectively. Also, hardness, ultimate tensile strength, yield strength, and elongation of AA2024–1 vol.%TiO<sub>2(np)</sub> composite were increased by about 25%, 28%, 4% and 163%, respectively, as compared to those of the monolithic component. The agglomerations of nanoparticles in the structure of nanocomposites were found to be a factor weakening the strength against the strengthening mechanisms. Some agglomerations of nanoparticles in the matrix were detected on the fractured surfaces of the tension test specimens.

**Key words:** AA2024–TiO<sub>2</sub> nanocomposites; mechanical properties; microstructure; fracture surface; stir casting process

## 1 Introduction

Metal matrix composites (MMCs) reinforced with micro-sized particles have been widely used in automotive and aerospace industries due to their high specific strength and modulus. However, the poor ductility of these MMCs restricts their use in many other applications [1–3]. Some recent research studies have suggested that the use of a small amount of nano-sized reinforcements not only improves the strength of the metallic alloys, but also, sometimes, significantly improves their ductility [4–6]. This has opened the horizons for the development of MMCs reinforced by nanoparticles, i.e. metal matrix nanocomposites (MMNCs). The interest in lightweight MMNCs has especially been growing in the recent years because of their high

specific strength.

The most widely used and cost-effective casting method for the production of MMCs and MMNCs is the stir casting (vortex casting) method. In this method, the reinforcing particles are introduced into the vortex formed on the melt surface by a high-speed stirrer drawing and dispersing them into the melt [1–3].

One of the main challenges in the production of nanocomposites by the stir casting technique is the wettability of nanoparticles and the melt [1–5]. Good wettability of nanoparticles with the molten matrix leads to the more effective dispersion and homogeneous distribution of nanoparticles in the matrix and better bonding of the reinforcement to the matrix; thus, better transfer of the load from the matrix to the reinforcement and improvement of the strengthening mechanisms could occur, resulting in

the better mechanical properties of the nanocomposite [3]. Different methods have been developed to overcome this problem. ABBASIPOUR et al [7], for instance, co-deposited Ni–P electroless coating and carbon nanotubes (CNTs) on aluminum powders were injected into the aluminum melt to improve the wettability of CNTs with the molten aluminum matrix. PAZHOUHANFAR and EGHBALI [8] also used  $K_2TiF_6$  to improve the wettability of micro-sized  $TiB_2$  particles with AA6061 melt using the stir casting method. The use of the in-situ processes in the production of MMCs by stir casting has been successfully examined, showing acceptable results in improving the wettability and distribution of particles in MMCs [9–11]. In some recent studies, the reinforcing particles were premixed with aluminum powder through low energy ball milling and the mixture was added to the molten matrix, where it was dissolved and gradually released into the melt. The results showed the improvement in the wettability and distribution of the reinforcing particles, as well as the enhancement in the mechanical properties of the produced MMCs [12–18]. In another work, SHAYAN et al [19,20] developed a hybrid method for the casting of A356–CNT nanocomposites. In this hybrid two-stage method, some initial Al–CNT composite stripes are made by an optimized accumulative roll bonding (ARB) process. Then, the composite stripes are dissolved and mechanically stirred in the molten A356 alloy; they are poured and solidified in a steel mold through the squeeze casting method. The dissolution of ARBed composite stripes under the surface of the melt and in the stirred liquid alloy also leads to the improvement in the wettability and distribution of CNTs in the composite matrix.

AA2024 aluminum alloy is a heat treatable aluminum alloy with copper as the main alloying element. The alloy is used where a high specific strength and a high fatigue strength are required. In addition to age hardening, the reinforcement of the alloy with ceramic nanoparticles can improve the applicability of the AA2024 alloy [2,21].

In the only published research on AA2024 matrix nanocomposites fabricated through ex-situ casting methods, HOZIEFA et al [22] produced the AA2024– $Al_2O_3$ (np) nanocomposite by the stir casting method. After that, they applied friction stir

processing on the casting nanocomposites to further improve the properties. They reported the improvement of the structural and mechanical properties of the matrix, as well as the elimination of the casting defects by adding the nanoparticles to the molten alloy. EL-MAHALLAWI et al [23–25] used  $TiO_2$  nanoparticles as the reinforcing phase in some Al–Si alloys, showing the improvement in the as-cast properties.

To the best of our knowledge, no published work is available on stir casting processing and characterization of  $TiO_2$  nanoparticles reinforced AA2024 aluminum matrix composites. Therefore, the innovation of the present work was the use of AA2024 as the matrix alloy and  $TiO_2$  nanoparticles as the reinforcement in the production of nanocomposites via the ex-situ stir casting method. More specifically, in this study, the objective was to produce AA2024– $TiO_2$ (np) nanocomposites by applying the stir casting method and characterize their properties.  $TiO_2$  nanoparticles were first mixed with Al and Cu powders; then the mixture was introduced to a molten AA2024 matrix by the stir casting method, and the microstructural and mechanical properties of the resulting nanocomposites were studied.

## 2 Experimental

$TiO_2$  nanoparticles with an average size of about 30 nm (from US Research Nanomaterials, Inc.) and the AA2024 aluminum ingot (from Iranian Aluminum Company (IRALCO), Iran) with the chemical composition shown in Table 1 were used as the reinforcing phase and matrix, respectively, for the casting of AA2024– $TiO_2$ (np) nanocomposites.  $TiO_2$  nanoparticles were mixed with the commercially pure (99.9%) Al powder (from GHATRAN SHIMI, Iran) and Cu powder (from GHATRAN SHIMI, Iran) with average sizes of 100 and 50  $\mu m$ , respectively, before adding them to the melt. Figure 1 shows the SEM images of the as-received powders.

**Table 1** Chemical composition of AA2024 matrix alloy (wt.%)

Fe	Cu	Mn	Mg	Ti	Sum of trace elements	Al
0.5	3.9	0.8	1.4	<0.1	0.7	Bal.

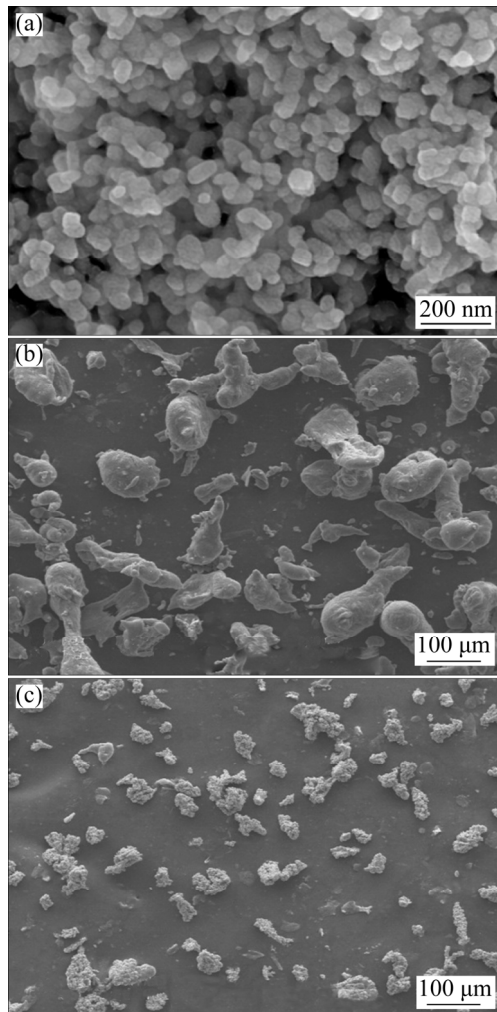


**Fig. 1** SEM images of as-received powders: (a)  $\text{TiO}_{2(\text{np})}$ ; (b) Al; (c) Cu

First, the desired quantity of  $\text{TiO}_2$  nanoparticles were mixed with appropriate amounts of Al (13.7 g) and Cu (2.2 g) powders in an ultra-low-energy ball mill with a ball-to-powder mass ratio of 5:1, a rotation speed of 60 r/min and a mixing time of 8 h. This would allow better dispersion and improved wettability of  $\text{TiO}_2$  nanoparticles in the matrix when they are added to the melt [12–18].

It is noteworthy that the amount of  $\text{TiO}_{2(\text{np})}$  in the powder mixture was about 40 vol.%. To examine the stability of  $\text{TiO}_2$  nanoparticles in the powder mixture and their potential reactions with the main alloying elements in the melt, the powder mixture was subjected to differential scanning calorimetry (DSC, STA L81 thermal analysis system) and X-ray diffraction analysis (XRD, Philips X'Pert PRO diffractometer).

The schematics of the casting set-up used

in the production of AA2024– $x\text{TiO}_{2(\text{np})}$  ( $x=0, 0.5, 1$  vol.%) nanocomposites can be seen in Fig. 2(a). This equipment included resistance furnace, alumina crucible with stopper, thermocouple, Ti impeller, argon gas entrance, reinforcing powder entrance and water-cooled steel mold. In each experiment, a measured quantity of the reinforcing powder mixture from the previous step was gradually added to the molten AA2024 aluminum alloy at 750 °C in 10 min. In order to protect the oxidation of the melt surface, argon gas was used. Melt stirring was performed using a titanium stirrer at 500 r/min. Stirring was continued for another 5 min after adding nanoparticles to the melt for the better dispersion of the nanoparticles. Then, the bottom stopper of the crucible was lifted and the composite slurry was poured into a water-cooled steel mold. The image of an actual cast sample and the nominal dimensions of the cast samples are shown in Figs. 2(b) and (c), respectively.

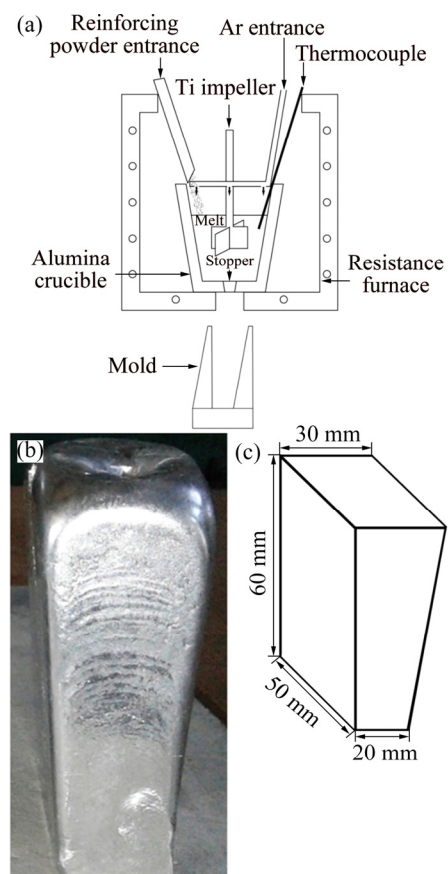


**Fig. 2** Schematics of casting set-up used (a), actual cast sample (b) and dimensions of cast samples (c)

The geometries of the casting, mold and water-cooling system were selected based on the simulation results obtained from ProCAST software

to minimize the casting defects and maximize the efficiency and solidification rate [26]. The mold was designed and positioned in such a way that during pouring, the melt flowed on the inclined inner wall of the mold and did not hit the mold bottom directly. This would minimize the turbulence in the melt and porosity formation in the casting. Previous studies have shown that higher solidification rates could increase the chance of the incorporation of nanoparticles in the solidification front [27,28].

It is worth noting that for the casting of the reference sample ( $x=0$ ), a completely similar procedure was performed except that the powder mixture added to the melt contained only Al and Cu powders without any  $\text{TiO}_2$  nanoparticles.

For structural and mechanical investigations, first, the castings were thoroughly washed and degreased; their densities were measured by using the Archimedes immersion method. Then, the castings were machined and sectioned along their heights into 9 specimens (Fig. 3). The middle specimens were etched with the Keller's solution and their microstructures were investigated using an optical microscope (Olympus BH2-UMA) connected to an image analysis system. Grain size and dendrite arm spacing (DAS) of the castings were measured using the ImageJ image analysis software according to the ASTM-E7 standard.  $\text{TiO}_2$  nanoparticles were studied using an FEI QUANTA FEG 450 field emission scanning electron microscope (FESEM) equipped with energy dispersive spectroscopy (EDS). The interface of the reinforcing nanoparticles and matrix of the nanocomposite was characterized using an FEI Tecnai  $G^2$  F20 transmission electron microscope

equipped with energy dispersive spectroscopy (EDS).

Brinell hardness of the samples was measured using a Wolpert Dia tester 2RC-S. Tensile test specimens with a gauge length of 20 mm and a gauge diameter of 4 mm were prepared according to the ASTM-E8M standard. Tensile tests were performed on a Hounsfield H50KH machine equipped with an extensometer at a crosshead speed of 1 mm/min. The resulting tensile fracture surfaces were examined by a Philips XI30 scanning electron microscope. Hardness and tensile tests for each casting were typically repeated five and three times, respectively, and their averages were reported. Scatter in the measurements was represented by error bars, showing the standard error of the mean of the measurements.

### 3 Results and discussion

#### 3.1 Powder mixture characterization

FESEM micrograph, XRD pattern and DSC curve of the reinforcing powder mixture prepared by ultra-low-energy ball milling are shown in Fig. 4. Figure 4(a) demonstrates the distribution of the nanoparticle agglomerates on the surface and among the metallic microparticles. GHAHREMANIAN et al [12,16] and AMIRKHANLOU and NIROUMAND [13–15,17,18] have successfully used this procedure for the dispersion of microsize reinforcements in aluminum melts. They have shown that by using this method, reinforcing particles are incorporated into the molten matrix more uniformly. GHAHREMANIAN et al [16] reported a reinforcement incorporation factor (RIF) of about 90% for this method.

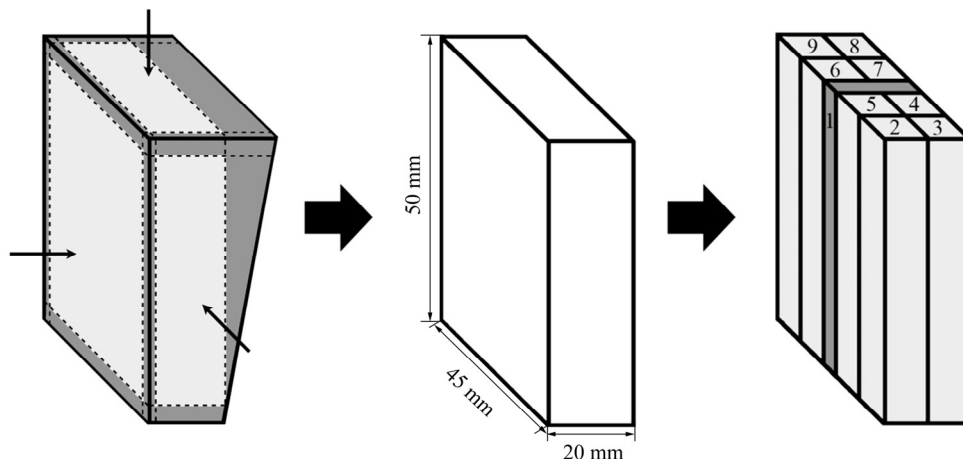
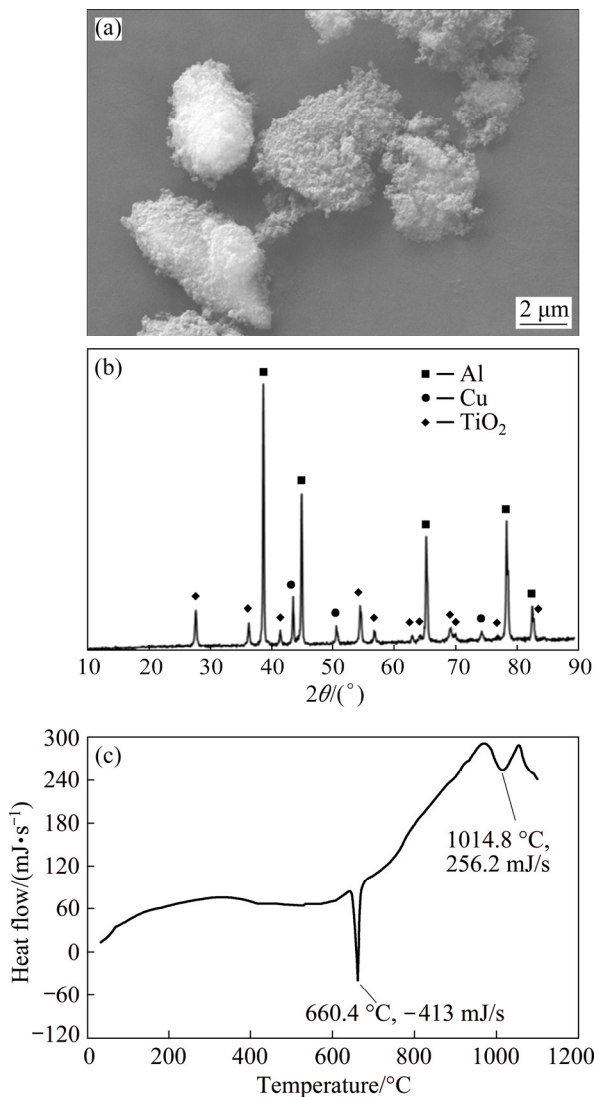


Fig. 3 Sample preparation sequences: 1—For structural investigations; 2–9—For mechanical properties investigations



**Fig. 4** Characteristics of ultra-low-energy ball milled reinforcing powder mixture: (a) FESEM micrograph; (b) XRD pattern; (c) DSC curve

X-ray diffraction pattern and DSC curve of the reinforcing powder mixture are shown in Figs. 4(b) and (c), respectively. It is evident that only the peaks corresponding to Al, Cu and  $\text{TiO}_2$  could be detected in the XRD pattern. There is not any peak related to new compounds other than Al, Cu, and  $\text{TiO}_2$  in the XRD pattern.

DSC analysis indicates only two endothermic peaks during heating the reinforcing powder mixture from the ambient temperature to 1100 °C. The first peak at 660.4 °C corresponds very well to the melting of the pure aluminum powder. The second one at 1014.8 °C corresponds to the melting of the copper powder at which the aluminum element has been partially diffused. The results

indicate no significant reaction between  $\text{TiO}_2$  nanoparticles and the metal powders up to 1100 °C.

Ellingham diagram shows that the oxidation free energy of Ti at all temperatures is higher than that of Al but lower than that of Cu [29]. Therefore, there is a thermodynamic driving force for the reaction of Al with  $\text{TiO}_2$  to form  $\text{Al}_2\text{O}_3$ , releasing some Ti in the molten matrix. The released Ti could result in the formation of the  $\text{TiAl}_3$  phase as well. In other words,  $\text{TiO}_2$  is expected to be unstable in contact with Al. However, several kinetic conditions must be met for these reactions to occur. For instance, mechanical activation, such as high intensity milling of the powder mixture facilitates the reaction [30–33]. In this study, the mixing operation using an ultra-low-energy ball milling was chosen to have no activation effect on the powder mixture. The DSC analysis suggests that no significant reaction was expected between the reinforcing nanoparticles and the metallic matrix during composite fabrication in this study.

### 3.2 Density

The measured densities of the castings are presented in Fig. 5. As shown, the density of the monolithic casting is more than that of the nanocomposites. Since the density of  $\text{TiO}_2$  (about 4 g/cm<sup>3</sup> [34,35]) is significantly higher than that of the matrix alloy used in this study (2.77 g/cm<sup>3</sup>), one would expect the opposite. However, the measured density is inversely proportional to the porosity content of the castings. The increased porosity could be the main reason for the lower density of the cast metal matrix composites [3]. Also, the higher density of the AA2024–1vol.% $\text{TiO}_2(\text{np})$

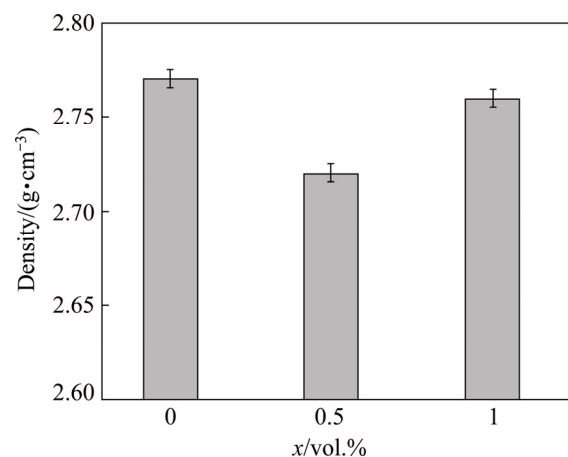


**Fig. 5** Densities of different castings of AA2024– $x\text{TiO}_2(\text{np})$

sample, as compared to that of the AA2024–0.5vol.%TiO<sub>2(np)</sub> sample, is clearly due to the higher density of TiO<sub>2(np)</sub>, in comparison with that of the matrix.

The increased porosity in metal matrix composites produced by the stir casting method has been reported by many researchers. Gas suction/entrapment from the melt surface being heavily stirred is one of the main sources of porosity formation in the stir cast metal matrix composites. Furthermore, oxide particles are generally known to be poorly wetted by metallic melts, providing suitable substrates for the nucleation of gas bubbles. Persistence of a gas layer around nanoparticles introduced to the melt as well as the tendency of nanoparticles to agglomerate aggravates the situation. The air entrapped in the agglomerates can expand heating inside the melt, producing more porosities. More difficult feeding of shrinkage porosities by the viscous composite slurry is another reason for the increased porosity in the metal matrix composites produced by liquid state methods [7,12–19,36].

### 3.3 Microstructure

The typical optical micrographs, as well as average grain size, dendrite arm spacing (DAS) and some observed porosities of the castings are shown in Fig. 6. More detailed microstructures showing

the interdendritic phases as well as the distribution of nanoparticles in the nanocomposite casting are presented in Fig. 6. As shown, all castings have equiaxed grain structures. While the average grain size of the monolithic casting is above 1200  $\mu\text{m}$ , and those of the nanocomposites are dropped by more than 66% to about 400  $\mu\text{m}$ . Furthermore, as suggested by the error bars in Fig. 6(d), the addition of the nanoparticles to the melt narrowed the grain size distribution in the nanocomposites samples. Figure 6(d) also showed that nanocomposites had smaller DAS, as compared to the monolithic casting, and their DAS was decreased as the TiO<sub>2</sub> content was increased. In fact, the DAS of AA2024–0.5vol.%TiO<sub>2(np)</sub> and AA2024–1vol.%TiO<sub>2(np)</sub> was decreased by about 19% and 31%, respectively, as compared to that of the monolithic casting.

Microstructural refinement by the addition of different reinforcements to aluminum melts has been frequently reported; it is generally associated with enhanced heterogeneous nucleation in the melt. Shear flow in the melt has also been reported to stimulate the heterogeneous nucleation sites which can refine the microstructure of the matrix alloy. On the other hand, the presence of nanoparticles is believed to lock the grain boundaries and prevent the excessive grain growth during cooling [7,19,37,38].

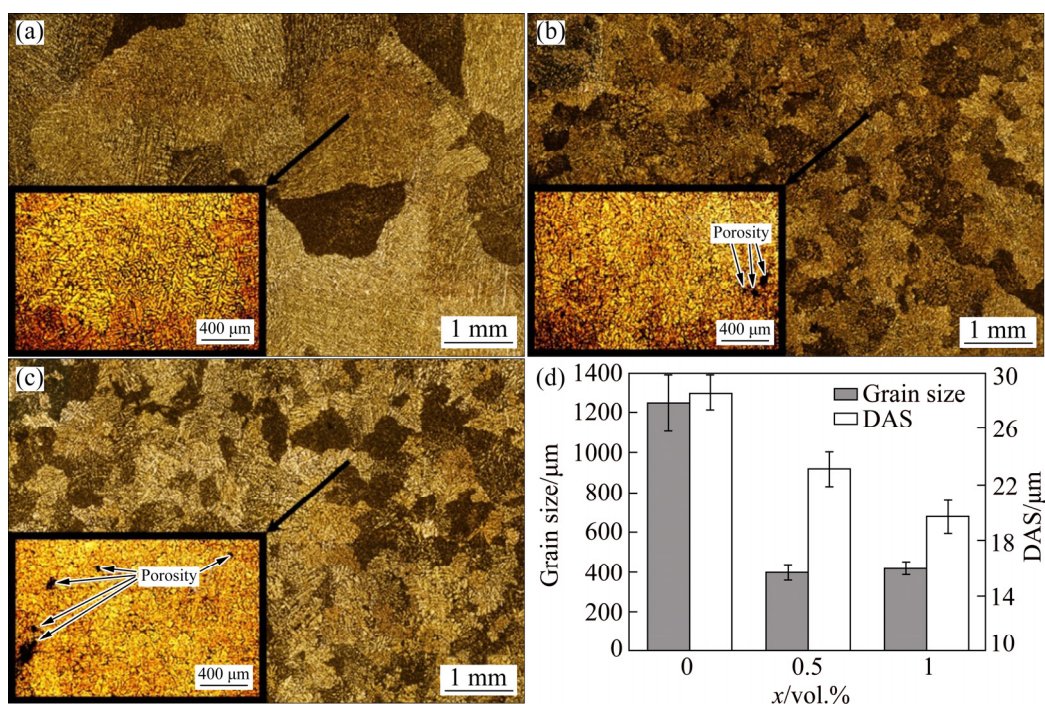


**Fig. 6** Microstructures of AA2024– $x$ TiO<sub>2(np)</sub> nanocomposites ( $x=0$  vol.% (a),  $x=0.5$  vol.% (b),  $x=1$  vol.% (c)) and grain size and dendrite arm spacing (DAS) as function of volume fraction of TiO<sub>2(np)</sub> (d)

FESEM micrographs of different castings and the TEM micrograph of the interface of the reinforcing nanoparticle and matrix of the nanocomposite with superimposed line scan EDS analysis are shown in Fig. 7. As can be seen in Figs. 7(a) and (b), the matrix structures in both monolithic and composite castings consist of  $\alpha(\text{Al})$  dendrites enclosed by a eutectic structure containing the eutectic  $\alpha(\text{Al})$  and some intermetallic phases. The most important intermetallic phases are  $\text{Al}_2\text{Cu}$  ( $\theta$ ) and  $\text{Al}_2\text{CuMg}$  ( $S$ ) [39]. Formation of the eutectic structure is an outcome of non-equilibrium solidification of the alloy, where solute elements with solute distribution coefficients ( $k_0$ ) less than unity are segregated in the residual melt between the growing dendrites. Solute segregation in the melt increases exponentially as the liquid fraction decreases until the composition and temperature of the interdendritic melt reach those of the eutectic transformation of the alloy. After that, the interdendritic melt maybe undergo a eutectic transformation in a very narrow temperature range when the interdendritic eutectic structure is formed. The difference between the nanocomposite sample and the monolithic sample lies in the presence of porosity due to the addition of reinforcing nanoparticles to the nanocomposite sample. The

reasons for these pores have already been addressed. These porosities could adversely affect the properties, especially the mechanical properties of the products, due to the elimination of continuity and uniformity of the matrix alloy [22].

Average chemical compositions of the  $\alpha(\text{Al})$  region in different samples measured from EDS analyses are presented in Table 2, revealing higher Ti and O contents in the nanocomposite samples, relative to the monolithic casting. This is obviously due to the incorporation of  $\text{TiO}_2$  nanoparticles in the composite castings, showing the effectiveness of the process employed in the fabrication of the composites.

Dispersion of  $\text{TiO}_2$  nanoparticles in the matrix of the cast nanocomposite is shown in Fig. 7(c). A careful examination of the microstructures revealed some agglomeration of the nanoparticles. White and black arrows in Fig. 7(c) point to some single and agglomerated  $\text{TiO}_2$  nanoparticles, respectively. The final distribution of nanoparticles in the composite is due to two sets of events. The first one happens during the dispersion of nanoparticles in the melt. In this case, the nanoparticles can settle to the bottom, float to the top surface or remain suspended in the melt, depending on many parameters such as their size, density difference with the melt, the type

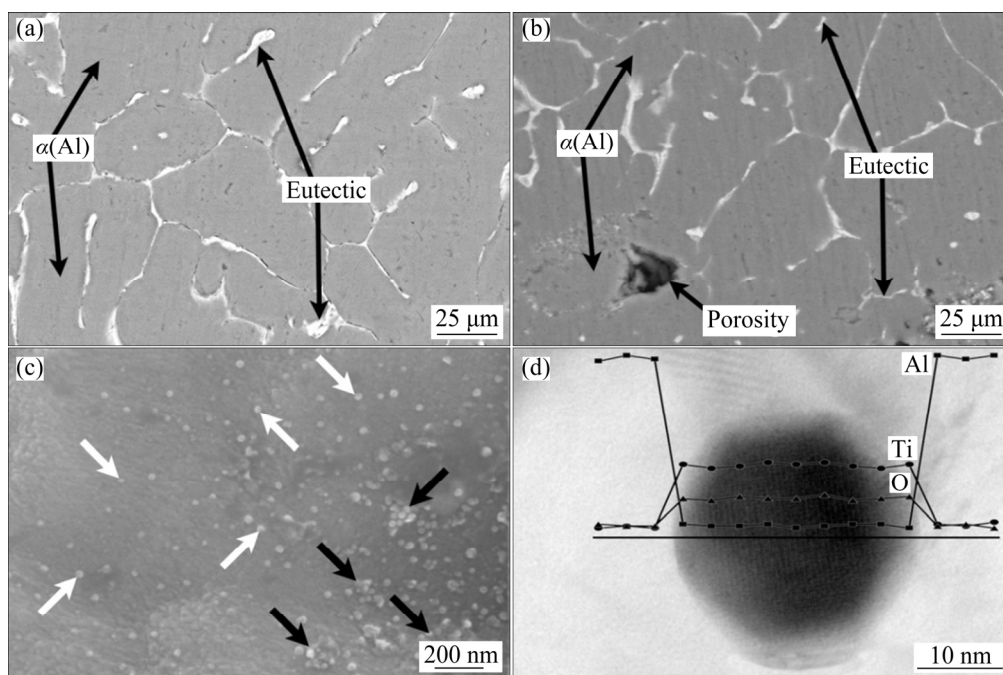


**Fig. 7** FESEM micrographs of AA2024- $x\text{TiO}_{2(\text{np})}$  castings ( $x=0$  vol.% (a),  $x=1$  vol.% (b),  $x=1$  vol.% at higher magnification (c)), and TEM micrograph of interface of  $\text{TiO}_{2(\text{np})}$  and matrix with superimposed line scan EDS analysis (d)

**Table 2** EDS analysis results of  $\alpha(\text{Al})$  region in different castings (wt.%)

Sample	Cu	Mn	Mg	Ti	O	Al
AA2024	4.9	1.8	3.5	0.1	1.0	88.7
AA2024– 0.5vol.%TiO <sub>2(np)</sub>	5.3	1.7	3.7	1.4	3.3	84.6
AA2024– 1 vol.%TiO <sub>2(np)</sub>	5.2	1.9	3.2	1.7	3.7	84.3

of the flow pattern induced in the crucible and the severity of stirring. Depending on the size of the suspended nanoparticles, their wettability with the melt and the effectiveness of the shearing action in the melt, the suspended particles may also agglomerate during the stir processing of the melt. The second set of events occur after casting the composite slurry in the mold due to the interplay between the solidification front and the reinforcing nanoparticles. Different researchers have shown that this behavior depends on several factors including the shape of the solidification front, solidification rate, nanoparticles volume fraction and temperature as well as the solute concentration gradients in the melt [3,40]. It has been shown that under any given set of processing conditions, a critical solidification front growth rate below which the solidification front pushes and above which the solidification front engulfs the suspended particles can be determined. This critical growth rate has an inverse relationship with the particle size [40,41].

Figure 7(c) shows the relatively uniform dispersion of the reinforcing particles in the matrix. This could be due to the provisions undertaken during the experimental procedure. Nanoparticles have a strong tendency to agglomerate due to their high surface modulus and consequently, their high zeta potential [42]. Obviously, the poor dispersion of the nanoparticles in the melt results in the poor distribution of the nanoparticles in the final composite. The advantages of premixing the nanoparticles with aluminum and copper powders are two sided. Although the bulk density of TiO<sub>2</sub> is higher than that of the molten matrix, in the nanopowder form, TiO<sub>2</sub> tends to float to the melt surface due to the entrapped air between the particles and its high specific surface area. The sinking of the added nanoparticles is facilitated by the presence of a heavy element such as copper in the powder mixture. On the other hand, premixing

the reinforcements with metallic particles reduces the initial agglomeration potential of the reinforcements, as well as providing for better dispersion when the metallic particles are melted in the molten matrix [14,16,17].

Furthermore, the bottom pouring arrangement employed (Fig. 2(a)) provides the continuous stirring of the composite slurry, even during casting of the slurry into the steel mold. Coupled with the high cooling rate in the water-cooled steel mold, this minimizes the time available for the agglomeration of the nanoparticles. It appears that the stirring process employed has not been able to provide the sufficient shear flow in the melt to break all agglomerates. Nevertheless, the detected agglomerates are generally not very large. It is known that increasing the stirring speed may improve the wettability and dispersion of the nanoparticles in the melt; however, at the same time, it may increase the porosity content of the castings [12]. Finally, the high solidification rate of the cast slurry in the water-cooled steel mold could increase the chances of the engulfment of the nanoparticles by the growing dendrites, resulting in their improved distribution in the solidified matrix.

The TEM micrograph of the nanocomposite with superimposed line scan EDS analysis is presented in Fig. 7(d). TEM micrograph of the interface, along with line scan EDS analysis, shows that the reinforcing nanoparticles are located in the matrix of the nanocomposite and these nanoparticles on the surface do not react with the metal matrix. As previously stated, the kinetic conditions for the reaction of oxide nanoparticles with molten aluminum are not provided.

### 3.4 Mechanical properties

Effects of the addition of TiO<sub>2</sub> nanoparticles to the AA2024 matrix on the hardness, ultimate tensile strength, yield strength and elongation of the alloy are shown in Fig. 8. Figure 8(b) represents the comparative true stress–true strain curves of different cast samples. It is evident that all mentioned properties were improved with the addition of TiO<sub>2</sub> nanoparticles. In fact, hardness, ultimate tensile strength, yield strength and elongation of the AA2024–1vol.%TiO<sub>2(np)</sub> composite were increased by about 25%, 28%, 4% and 163%, respectively, as compared to those of the monolithic casting. The improvement in the elongation value is

striking since, normally, the increase in the hardness and strength of metal matrix composites happens at the expense of their ductility [1].

It appears that microstructural refinement serves a vital role in the improvement of the mechanical properties of the nanocomposites. Grain refinement provides more grain boundaries and obstacles to dislocation movement and enhances the strength [19,43]. As shown in Fig. 6(d), the average grain size of the cast nanocomposites is 66% smaller than that of the monolithic casting. The increase in the yield strength by grain refinement could be quantified through the Hall–Patch equation, indicating an inverse square root relationship between the yield strength and the grain size, at least for the micrometer scale grain size [3].

Furthermore, it has been shown that the incorporation of nanoparticles to a metallic matrix results in the generation of a series of geometrically necessary dislocations due to the CTE (coefficient of thermal expansion) mismatch of the particles and the matrix induced during cooling from the high to ambient temperature in the production process. This can result in work hardening during mechanical

tests. Secondly, by creating obstacles to the dislocations motion, the reinforcing particles increase the threshold stress required for dislocations mobility and strengthen the nanocomposite [43,44].

Another strengthening mechanism is the Orowan mechanism, by which non-shearable ceramic reinforcement particles pin the moving dislocations, leading to dislocations bowing around particles under an external load [5,40]. The effect of the mechanism is inversely proportional to the average spacing between the reinforcing particles; therefore, the degree of strengthening is believed to be insignificant for micro-sized reinforcements. Uniform dispersion and limited agglomeration of  $\text{TiO}_2$  nanoparticles in this study, as shown in Fig. 7, could result in a larger number of effective dispersed non-shearable points and smaller spacing between them would favor the promotion of the Orowan mechanism.

As previously stated, the agglomeration of nanoparticles and formation of porosity are two downsides of the liquid state processing for the manufacturing of metal matrix composites. These could result in poor structural and mechanical

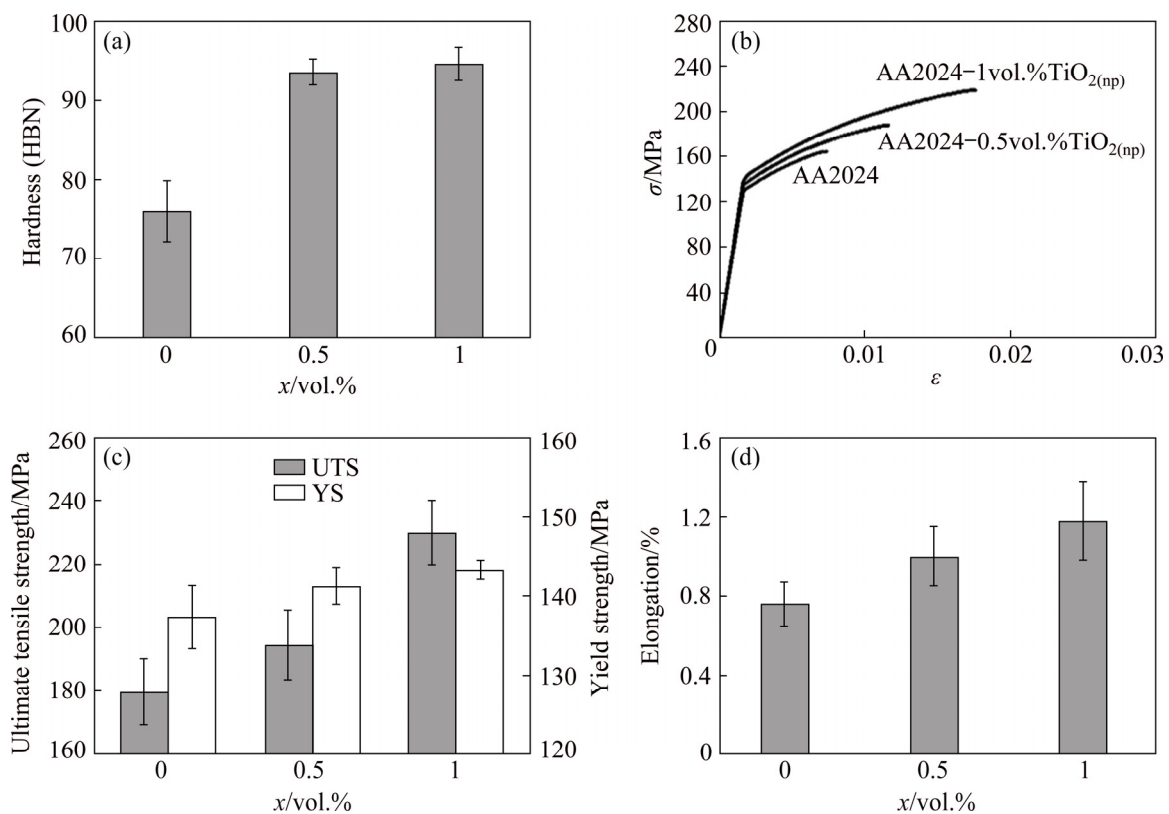


**Fig. 8** Mechanical properties of different AA2024- $x\text{TiO}_{2(\text{np})}$  castings: (a) Hardness; (b) True stress–true strain curves; (c) Ultimate tensile and yield strengths; (d) Elongation

properties. The presence of porosity could reduce the load tolerance in the matrix. In this case, the porous areas will be yielded first through strain concentration. On the other hand, the presence of pores creates a multi-axis stress state, leading to the local strain concentration in the adjacent matrix [45,46]. Two types of operations improve the distribution of nanoparticles in the microstructure of nanocomposites produced via the stir casting process. One is the operation used during the stirring and casting process. The use of ultrasonic waves is part of this category. It has been shown that the use of ultrasonic waves through the stir casting process plays an effective role in improving the microstructure and distribution of ceramic nanoparticles and preventing them from clustering [6,47–50]. This phenomenon, resulting from the entry of high energy ultrasonic waves, includes acoustic streaming and ultrasonic cavitation; preventing the nanoparticles from sticking together. These could lead to the modification of the more uniform reinforcement's dispersion in the metal matrix [6]. The other is the operation used after the stir casting process. Subsequent mechanical operations located in this category are useful. In order to reduce porosity and particles agglomeration in the cast metal matrix composites, the use of subsequent mechanical processes such as accumulative roll bonding has been successfully examined before [51–54]. This is the subject of our future work.

### 3.5 Fractography

Figure 9 shows micrographs of the fracture surfaces of the tensile test specimens of different castings. Figure 9(a) exhibits that the failure of the monolithic casting is brittle and intergranular. Some intact and broken dendrites could be clearly seen along with some cleavage planes in the fracture surface. This type of failure is in agreement with the low elongation values of the monolithic sample in the tension tests as shown in Fig. 8.

The micrographs of tensile fracture surfaces of the nanocomposite castings are shown in Figs. 9(b) and (c). Some of the large  $\text{TiO}_2$  agglomerates observed on the fracture surface are marked by black arrows in the figures. Figures 9(b) and (c) indicate that the failure in composite castings is also brittle, though of the transgranular type. It seems that the presence of  $\text{TiO}_2$  nanoparticles changed the

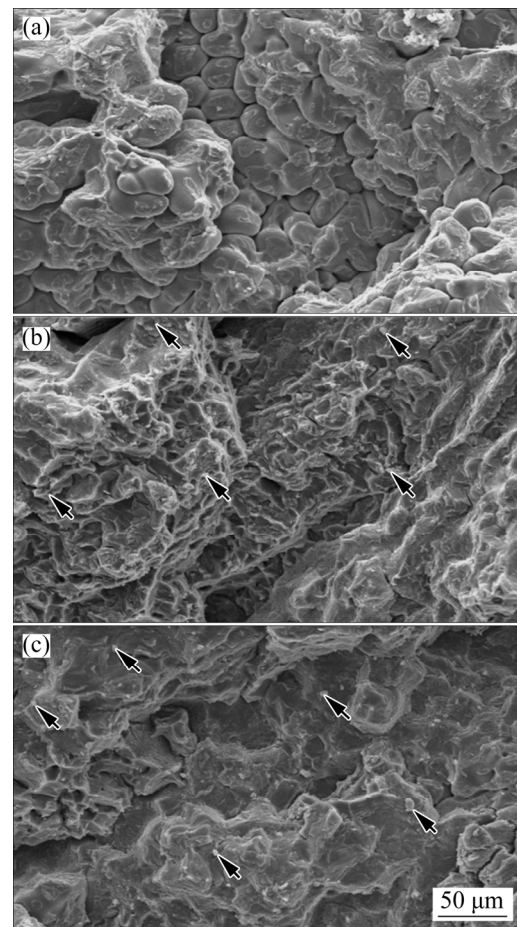


**Fig. 9** Micrographs tensile fracture surfaces of different AA2024- $x\text{TiO}_{2(\text{np})}$  cast composites: (a)  $x=0$  vol.%; (b)  $x=0.5$  vol.%; (c)  $x=1$  vol.%

fracture behavior of the castings from the intergranular mode to transgranular one. The existence of cleavage planes, some porosities, tensile stress-induced cracks and the increase of strain are evident in the fracture surface of the composite castings.

The number and size of cracks in AA2024-0.5vol.% $\text{TiO}_{2(\text{np})}$ , rather than AA2024-1vol.% $\text{TiO}_{2(\text{np})}$ , are much larger and smaller, respectively. So, the nucleation of cracks in AA2024-0.5vol.% $\text{TiO}_{2(\text{np})}$  is greater than that of AA2024-1vol.% $\text{TiO}_{2(\text{np})}$ . On the contrary, the crack growth in AA2024-1vol.% $\text{TiO}_{2(\text{np})}$  is higher than that of AA2024-0.5vol.% $\text{TiO}_{2(\text{np})}$ . The fracture surface in AA2024-1vol.% $\text{TiO}_{2(\text{np})}$  has fewer cleavage planes with larger dimensions in comparison with that of the AA2024-0.5vol.% $\text{TiO}_{2(\text{np})}$ . The greater elongation of AA2024-1vol.% $\text{TiO}_{2(\text{np})}$  rather than AA2024-0.5vol.% $\text{TiO}_{2(\text{np})}$  is due to the two recent phenomena.

## 4 Conclusions

(1) AA2024- $x$ TiO<sub>2(np)</sub> ( $x=0, 0.5, 1$  vol.%) nanocomposites were produced by the stir casting method.

(2) The characterization of the reinforcing powder mixture indicated that there was no reaction between nanoparticles and the melt.

(3) The microstructural changes due to the fabrication of nanocomposites were the reductions in grain size and dendrite arm spacing, the distribution of reinforcing nanoparticles, the presence of nanoparticles agglomerations, and the increased porosity.

(4) The mechanical properties of the products were improved by adding TiO<sub>2</sub> nanoparticles to the matrix alloy. The developments in mechanical properties were due to some strengthening mechanisms.

(5) The analysis of fractographs revealed that the failure of the monolithic casting was of brittle and interdendritic type and that of composite castings was of brittle and transgranular one.

## References

- [1] RAY S. Review of cast metal matrix particulate composite [J]. *Journal of Materials Science*, 1993, 28: 5397–5413.
- [2] CLYNE T W, WITHERS P J. An introduction to metal matrix composites [M]. Cambridge: Cambridge University Press, 1993.
- [3] CHAWALA N, CHAWLA K K. Metal matrix composites [M]. 2nd ed. Heidelberg: Springer, 2006.
- [4] THOSTENSON E T, LI C, CHOU T W. Nanocomposites in context [J]. *Composites Science and Technology*, 2005, 65: 491–516.
- [5] CASATI R, VEDANI M. Metal matrix composites reinforced by nano-particles—A review [J]. *Metals*, 2014, 4: 56–83.
- [6] DEHNAVI M R, NIROUMAND B, ASHRAFIZADEH F, ROHATGI P K. Effects of continuous and discontinuous ultrasonic treatments on mechanical properties and microstructural characteristics of cast Al413-SiC<sub>np</sub> nanocomposite [J]. *Materials Science and Engineering A*, 2014, 617: 73–83.
- [7] ABBASIPOUR B, NIROUMAND B, MONIRVAGHEFI S M. Compcasting of A356-CNT composite [J]. *Transactions of Nonferrous Metals Society of China*, 2010, 20: 1561–1566.
- [8] PAZHOUHANFAR Y, EGHBALI B. Microstructural characterization and mechanical properties of TiB<sub>2</sub> reinforced Al6061 matrix composites produced using stir casting process [J]. *Materials Science and Engineering A*, 2018, 710: 172–180.
- [9] MALEKI A, MERATIAN M, NIROUMAND B, GUPTA M. Synthesis of in-situ aluminum matrix composite using a new activated powder injection method [J]. *Metallurgical and Materials Transactions A*, 2008, 39: 3034–3039.
- [10] SENEMAR M, MALEKI A, NIROUMAND B, ALLAFCHIAN R. A Novel and facile method for silica nanoparticles synthesis from high temperature vulcanization (HTV) silicon [J]. *Metallurgical and Materials Engineering*, 2017, 22: 1–8.
- [11] BOROONI M, NIROUMAND B, MALEKI A. Synthesis and characterization of in-situ magnesium based cast nano composite via nano-SiO<sub>2</sub> addition to the melt [J]. *Materials and Technology*, 2017, 51: 945–951.
- [12] GHAREMANIAN M, NIROUMAND B. Compcasting of an Al-Si-SiC<sub>p</sub> composite using powder injection method [J]. *Solid State Phenomena*, 2008, 141–143: 175–180.
- [13] AMIRKHANLOU S, NIROUMAND B. Synthesis and characterization of Al356-SiC<sub>p</sub> composites by stir casting and compcasting methods [J]. *Transactions of Nonferrous Metals Society of China*, 2010, 20: 788–793.
- [14] AMIRKHANLOU S, NIROUMAND B. Development of Al356/SiC<sub>p</sub> cast composites by injection of SiC<sub>p</sub> containing composite powders [J]. *Materials and Design*, 2011, 32: 1895–1902.
- [15] AMIRKHANLOU S, NIROUMAND B. Effects of reinforcement distribution on low and high temperature tensile properties of Al356/SiC<sub>p</sub> cast composites produced by a novel reinforcement dispersion technique [J]. *Materials Science and Engineering A*, 2011, 528: 7186–7195.
- [16] GHAREMANIAN M, NIROUMAND B, PANJEPOUR M. Production of Al-Si-SiC<sub>p</sub> cast composites by injection of low-energy ball-milled Al-SiC<sub>p</sub> powder into the melt [J]. *Journal of Metals and Materials International*, 2012, 18: 149–156.
- [17] AMIRKHANLOU S, NIROUMAND B. Fabrication and characterization of Al356/SiC<sub>p</sub> semisolid composites by injecting SiC<sub>p</sub> containing composite powders [J]. *Journal of Materials Processing Technology*, 2012, 212: 841–847.
- [18] AMIRKHANLOU S, NIROUMAND B. Microstructure and mechanical properties of Al356/SiC<sub>p</sub> cast composites fabricated by a novel technique [J]. *Journal of Materials Engineering and Performance*, 2013, 22: 85–93.
- [19] SHAYAN M, NIROUMAND B. Synthesis of A356-MWCNT nanocomposites through a novel two stage casting process [J]. *Materials Science and Engineering A*, 2013, 582: 262–269.
- [20] SHAYAN M, NIROUMAND B, TOROGHINEJAD M R. Effect of applied pressure on mechanical properties of squeeze cast Al-MWCNT composites [C]// *Materials Science and Technology Conference and Exhibition 2012, MS and T 2012*. Pittsburgh, Pennsylvania, USA, 2012: 128–135.
- [21] KAÇAR H, ATIK E, MERİÇ C. The effect of precipitation-hardening conditions on wear behaviours at 2024 aluminium wrought alloy [J]. *Journal of Materials Processing Technology*, 2003, 142: 762–766.
- [22] HOZIEFA W, TOSCHI S, AHMED M M Z, MORRI AI, MAHDY A A, EL-SAYED SELEMAN M M,

- EL-MAHALLAWI I, CESCHINI L, ATLAM A. Influence of friction stir processing on the microstructure and mechanical properties of a compocast AA2024–Al<sub>2</sub>O<sub>3</sub> nanocomposite [J]. *Materials and Design*, 2016, 106: 273–284.
- [23] EL-MAHALLAWI I, SHASH Y, EIGENFELD K, MAHMOUD T S, RAGAIE R M, SHASH A Y, EL-SAEED M A. Influence of nanodispersions on strength–ductility properties of semisolid cast A356 Al alloy [J]. *Materials Science and Technology*, 2010, 26: 1226–1231.
- [24] EL-MAHALLAWI I, SHASH Y, RASHAD R M, ABDELAZIZ M H, MAYER J, SCHWEDT A. Hardness and wear behaviour of semi-solid cast A390 alloy reinforced with Al<sub>2</sub>O<sub>3</sub> and TiO<sub>2</sub> nanoparticles [J]. *Arabian Journal for Science and Engineering*, 2014, 39: 5171–5184.
- [25] EL-MAHALLAWI I, SHASH Y, AMER A E. Nanoreinforced cast Al–Si alloys with Al<sub>2</sub>O<sub>3</sub>, TiO<sub>2</sub> and ZrO<sub>2</sub> nanoparticles [J]. *Metals*, 2015, 5: 802–821.
- [26] SHAYAN M, EGHBALI B, NIROUMAND B, LASHANI ZAND M. Casting and mould design of as cast Al2024 alloy using ProCAST software [C]//Proceedings of the 5th International Conference on Materials Engineering and Metallurgy. Shiraz, Iran, 2016.
- [27] HASHIM J, LOONEY L, HASHMI M S J. Particle distribution in cast metal matrix composites—Part I [J]. *Journal of Materials Processing Technology*, 2002, 123: 251–257.
- [28] HASHIM J, LOONEY L, HASHMI M S J. Particle distribution in cast metal matrix composites—Part II [J]. *Journal of Materials Processing Technology*, 2002, 123: 258–263.
- [29] STRATTON P. Ellingham diagrams—Their use and misuse [J]. *International Heat Treatment and Surface Engineering*, 2013, 7: 70–73.
- [30] FUKUNAGA H, WANG X, ARAMAKI Y. Preparation of intermetallic compound matrix composites by reaction squeeze casting [J]. *Journal of Materials Science Letters*, 1990, 9: 23–25.
- [31] PENG H X, WANG D Z, GENG L, YAO C K, MAO J F. Evaluation of the microstructure of in-situ reaction processed Al<sub>3</sub>Ti–Al<sub>2</sub>O<sub>3</sub>–Al composite [J]. *Scripta Materialia*, 1997, 37: 199–204.
- [32] MALEKI A, PANJEPOUR M, NIROUMAND B, MERATIAN M. Mechanism of zinc oxide–aluminum aluminothermic reaction [J]. *Journal of Materials Science*, 2010, 45: 5574–5580.
- [33] MALEKI A, HOSSEINI N, NIROUMAND B. A review on aluminothermic reaction of Al/ZnO system [J]. *Ceramics International*, 2018, 44: 10–23.
- [34] MAZAHERI M, ZAHEDI A M, HAGHIGHATZADEH M, SADRNEZHAAD S K. Sintering of titania nanoceramic: Densification and grain growth [J]. *Ceramics International*, 2009, 35: 685–691.
- [35] MARINEL S, CHOI D H, HEUGUET R, AGRAWAL D, LANAGAN M. Broadband dielectric characterization of TiO<sub>2</sub> ceramics sintered through microwave and conventional processes [J]. *Ceramics International*, 2013, 39: 299–306.
- [36] EZATPOUR H R, SAJJADI S A, HADDAD SABZEVAR M, HUANG Y. Investigation of microstructure and mechanical properties of Al6061-nanocomposite fabricated by stir casting [J]. *Materials and Design*, 2014, 55: 921–928.
- [37] HAGHAYEGHI R, NASTAC L. On microstructural refinement of an AA7449 aluminium alloy through shearing above liquidus temperature [J]. *Materials Letters*, 2011, 65: 3230–3233.
- [38] MOHAMMADI BADIZI R, ASKARI-PAYKANI M, PARIZAD A, SHAHVERDI H R. Effects of electromagnetic frequency and SiC nanoparticles on the microstructure refinement and mechanical properties of Al A357–1.5wt.%SiC nanocomposites [J]. *International Journal of Metalcasting*, 2018, 12: 565–573.
- [39] WANG S C, STARINK M J. Precipitates and intermetallic phases in precipitation hardening Al–Cu–Mg–(Li) based alloys [J]. *International Materials Reviews*, 2005, 50: 193–215.
- [40] ETEMADI R, WANG B, PILLAI K M, NIROUMAND B, OMRANI E, ROHATGI P. Pressure infiltration processes to synthesis metal matrix composites—A review of metal matrix composites, the technology and process simulation [J]. *Materials and Manufacturing Processes*, 2018, 33: 1261–1290.
- [41] FRAS E, OLEJNIK E. Interaction between solidification front and alien phase particles [J]. *Archives of Metallurgy and Materials*, 2008, 53: 695–702.
- [42] RANA R S, PUROHIT R, SONI S, DAS S. Comparison of mechanical properties and microstructure of aluminum alloy micron and nano SiC composites fabricated by ultrasonic vibration [J]. *International Journal of Advance Engineering and Research Development*, 2014, 1–12: 135–146.
- [43] SHAYAN M, EGHBALI B, NIROUMAND B. Synthesis of AA2024–(SiO<sub>2np</sub>+TiO<sub>2np</sub>) hybrid nanocomposite via stir casting process [J]. *Materials Science and Engineering A*, 2019, 756: 484–491.
- [44] ZHANG Z, TOPPING T, LI Y, VOGT R, ZHOU Y, HAINES C, PARAS J, KAPOOR D, SCHOENUNG J M, LAVERNIA E J. Mechanical behavior of ultrafine-grained Al composites reinforced with B<sub>4</sub>C nanoparticles [J]. *Scripta Materialia*, 2011, 65: 652–655.
- [45] ZHANG L B, JINTAO L, YANWEN W. Plastic working and superplasticity in aluminium–matrix composites reinforced with SiC particulates [J]. *Journal of Materials Processing Technology*, 1998, 84: 271–273.
- [46] TEKMEK C, OZDEMIR I, COCEN U, ONEL K. The mechanical response of Al–Si–Mg/SiC<sub>p</sub> composite: Influence of porosity [J]. *Materials Science and Engineering A*, 2003, 360: 365–371.
- [47] KHANDELWAL A, MANI K, SRIVASTAVA N, GUPTA R, CHAUDHARI G P. Mechanical behavior of AZ31/Al<sub>2</sub>O<sub>3</sub> magnesium alloy nanocomposites prepared using ultrasound assisted stir casting [J]. *Composites Part B: Engineering*, 2017, 123: 64–73.
- [48] MADHUKAR P, SELVARAJ N, GUJJALA R, RAO C S P. Production of high performance AA7150–1%SiC nanocomposite by novel fabrication process of ultrasonication assisted stir casting [J]. *Ultrasonics Sonochemistry*, 2019, 58: 104665.
- [49] MADHUKAR P, SELVARAJ N, RAO C S P, KUMAR G B

- V. Fabrication and characterization two-step stir casting with ultrasonic assisted novel AA7150–hBN nanocomposites [J]. *Journal of Alloys and Compounds*, 2020, 815: 152464.
- [50] MOHANTY P, MAHAPATRA R, PADHI P, RAMANA C V V, MISHRA D K. Ultrasonic cavitation: An approach to synthesize uniformly dispersed metal matrix nanocomposites —A review [J]. *Nano-Structures & Nano-Objects*, 2020, 23: 100475.
- [51] AMIRKHANLOU S, JAMAATI R, NIROUMAND B, TOROGHINEJAD M R. Fabrication and characterization of Al/SiC<sub>p</sub> composites by CAR process [J]. *Materials Science and Engineering A*, 2011, 528: 4462–4467.
- [52] JAMAATI R, AMIRKHANLOU S, TOROGHINEJAD M R, NIROUMAND B. Effect of particle size on microstructure and mechanical properties of composites produced by ARB process [J]. *Materials Science and Engineering A*, 2011, 528: 2143–2148.
- [53] AMIRKHANLOU S, REZAEI M, NIROUMAND B, TOROGHINEJAD M R. Refinement of microstructure and improvement of mechanical properties of Al/Al<sub>2</sub>O<sub>3</sub> composite by accumulative roll bonding process [J]. *Materials Science and Engineering A*, 2011, 528: 2548–2553.
- [54] SHAYAN M, EGHBALI B, NIROUMAND B. The role of accumulative roll bonding after stir casting process to fabricate high-strength and nanostructured AA2024–(SiO<sub>2</sub>+TiO<sub>2</sub>) hybrid nanocomposite [J]. *Journal of Alloys and Compounds*, 2020, 845: 156281.

## 搅拌铸造法制备 AA2024–TiO<sub>2</sub> 纳米复合材料

Mehrdad SHAYAN<sup>1</sup>, Beitallah EGHBALI<sup>1</sup>, Behzad NIROUMAND<sup>2</sup>

1. Department of Materials Science and Engineering, Sahand University of Technology,

P. O. Box 51335-1996, Tabriz, Iran;

2. Department of Materials Engineering, Isfahan University of Technology, Isfahan 84156-83111, Iran

**摘要:** 考虑到在非原位铸造法制备复合材料时不使用 TiO<sub>2</sub> 纳米颗粒作为 AA2024 合金的增强相, 采用搅拌铸造法制备 AA2024–x%TiO<sub>2(np)</sub> (x=0, 0.5%, 1%, 体积分数) 纳米复合材料。利用光学显微镜和扫描电子显微镜研究样品的结构性能, 并采用硬度和拉伸试验研究其力学性能。结果表明, 添加 1% TiO<sub>2</sub>(体积分数) 纳米颗粒后, 样品的晶粒尺寸和枝晶臂间距分别减小约 66% 和 31%; 硬度、抗拉强度、屈服强度和伸长率分别提高约 25%、28%、4% 和 163%。在拉伸试样的断口表面观察到团聚在基体中的纳米颗粒。纳米复合材料结构中纳米颗粒的团聚是其强度在强化机制下减弱的因素。

**关键词:** AA2024–TiO<sub>2</sub> 纳米复合材料; 力学性能; 显微组织; 断裂表面; 搅拌铸造工艺

(Edited by Wei-ping CHEN)